γ-Band deficiency and abnormal thalamocortical activity in P/Q-type channel mutant mice

Rodolfo R. Llinás*†, Soonwook Choi*‡§, Francisco J. Urbano*¶, and Hee-Sup Shin†‡§

*Department of Physiology and Neuroscience, New York University School of Medicine, 550 First Avenue, New York, NY 10016; ‡Center for Neural Science, Korea Institute of Science and Technology, Seoul 136-791, Korea; §Department of Neuroscience, University of Science and Technology, Daejon 305-333, Korea; and ¶Laboratotio de Fisiología y Biología Molecular, Instituto de Fisiología, Biología Molecular y Neurociencias, Universidad de Buenos Aires–Consejo Nacional de Investigaciones Científicas y Técnicas de Argentina, Ciudad Universitaria, C1428EHA Buenos Aires, Argentina

Contributed by Rodolfo R. Llinas, September 4, 2007 (sent for review June 7, 2007)

Thalamocortical *in vivo* and *in vitro* function was studied in mice lacking P/Q-type calcium channels ($Ca_V2.1$), in which N-type calcium channels ($Ca_V2.2$) supported central synaptic transmission. Unexpectedly, *in vitro* patch recordings from thalamic neurons demonstrated no γ-band subthreshold oscillation, and voltage-sensitive dye imaging demonstrated an absence of cortical γ-band-dependent columnar activation involving cortical inhibitory interneuron activity. *In vivo* electroencephalogram recordings showed persistent absence status and a dramatic reduction of γ-band activity. Pharmacological block of T-type calcium channels (Ca_V3), although not noticeably affecting normal control animals, left the knockout mice in a coma-like state. Hence, although N-type calcium channels can rescue P/Q-dependent synaptic transmission, P/Q calcium channels are essential in the generation of γ-band activity and resultant cognitive function.

1-Octanol | patch clamp | VSDI | electroencephalogram | calcium channel

Voltage-gated calcium channels (VGCCs) play a central role in determining intrinsic neuronal properties (1–3) and mediating calcium-dependent synaptic transmission (4). Since its first description using pharmacological tools (5), P-type channels (presently known as P/Q or $Ca_V2.1$ channels) have been found to be widely distributed in CNS neurons (6, 7). They also are responsible for the Ca^{2+} entry that triggers synaptic transmission at a majority of synapses in the mammalian CNS (5, 7). These channels are characterized by the pore-forming α-1A subunit (with support from ancillary subunits) and are engaged in close interactions with the SNARE complex at the release machinery (3, 8). Moreover, such reciprocal interactions are a prerequisite for the normal functioning of P/Q-type calcium channels (9, 10).

In the thalamocortical system, P/Q-type VGCCs located in the dendrites of neurons support the characteristic 35- to 45-Hz γ-band oscillations. This activity, considered to be a functional prerequisite to cognitive states, is present at both the network (11, 12) and neuronal levels as subthreshold oscillations (13–15). P/Q-type channels also mediate glutamatergic and GABAergic synaptic transmission in the cortex and thalamus (16, 17). Indeed, mutations of different subunits of the P/Q-type channel can induce alterations in both GABAergic and glutamatergic synaptic transmission in the thalamocortical system (18–20) and, thus, provide a good example of the central role of calcium conductances in thalamocortical physiology.

Transitions between γ-band oscillations (associated with wakefulness and consciousness) and low-frequency bursts (associated with somnolence and sleep) occur rapidly (21, 22). During such transitions, the dynamic and differential activations of both P/Q- and T-type calcium channels are necessary. Indeed, aberrations in these thalamocortical dynamics also may serve as the basis for a class of neurological and neuropsychiatric disorders that can be grouped under the name "thalamocortical dysrhythmia syndrome" (23, 24).

A murine model lacking $Ca_V2.1$ VGCC has been described as suffering from several neurological problems (25). Indeed, near postnatal day (P) 10, the animals begin to have difficulty walking, have absence seizures, and are ataxic and dystonic. These problems become more acute with age until the mice are unable to walk and die at $\approx$3 weeks of age. Although the reason for their death is multifactorial, including inanition, synaptic transmission deficits clearly play a central role. Although other types of VGCCs support synaptic transmission in these mutant animals (25–28), clear deficiencies were observed in the dynamics of synaptic transmission that are related to changes in the presynaptic calcium current (26, 29, 30). There also is an increment in the density of T-type VGCCs that support low-threshold (LVA) action potentials in the absence of P/Q channels (30). As described here, the increased presence of T-type channel expression in thalamocortical neurons is causally related to the generation of absence seizures.

Here we address the hypothesis that the neurological problems present in mice lacking $Ca_V2.1$ VGCCs are linked to the fact that P/Q-type VGCCs are irreplaceable for normal thalamocortical function. Moreover, it is proposed that, although P/Q-type channels are central to the generation of cognitive states, T-type channels mediate sleep thalamocortical dynamics.

To test this hypothesis, we combined results from *in vitro* voltage-sensitive dye imaging (VSDI) and patch-clamp recordings with *in vivo* electroencephalograms (EEGs). These findings may be grouped into four key observations: (*i*) $Ca_V2.2$, N-type VGCCs mediated synaptic transmission in both thalamocortical and corticothalamic synapses; (*ii*) the typical pattern activated by 40-Hz subcortical white matter stimulation (i.e., cortical columnar activation flanked by inhibition) found in *in vitro* slices from wild-type (WT) mice was not elicited in slices from knockout (KO) mice (31); (*iii*) subthreshold γ-band oscillations were not present in thalamic neurons; and (*iv*) when T-type VGCCs were partially blocked, the animals entered a coma-like state. Taken together, these findings indicate that P/Q channels are essential for the generation of γ-band activity and cognition-related thalamocortical functional states.

Results

Thalamocortical activity was initially studied in slices from $Ca_V2.1$-null mice (KO), their WT, and heterozygous $Ca_V2.1$-null littermates. The heterozygous mice had the same phenotype as previously described (25, 26) and were combined with the WT into one control group, which here are called WT. We used thalamocortical slices in combination with VSDI to study the patterns of both putamen/striatum and cortical activities while stimulating ventrobasal (VB) thalamic nucleus at both 40- and 10-Hz frequencies. The

Author contributions: R.R.L. designed research; R.R.L., S.C., and F.J.U. performed research; H.-S.S. contributed new reagents/analytic tools; R.R.L., S.C., and F.J.U. analyzed data; and R.R.L., F.J.U., and H.-S.S. wrote the paper.

The authors declare no conflict of interest.

Freely available online through the PNAS open access option.

†To whom correspondence may be addressed. E-mail: llinar01@med.nyu.edu or heesup.shin@gmail.com.

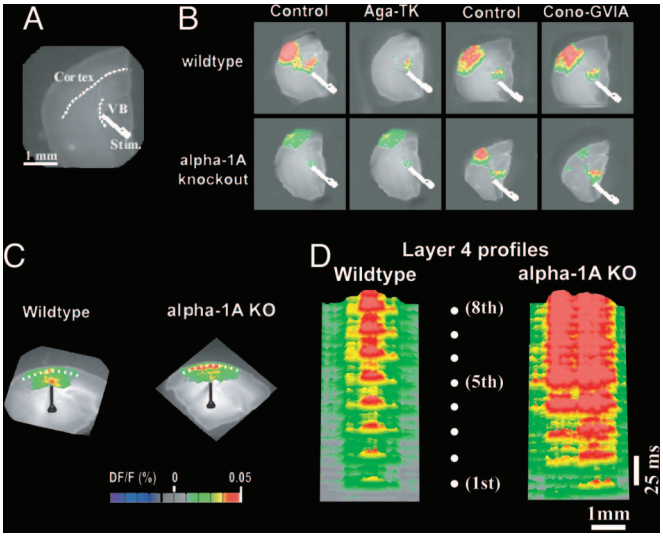

Fig. 1. P/Q-type VGCCs' replacement by N-channels in KO mice induces absence of cortical columnar activation as shown by VSDI. (*A*) Phase-contrast photo of a thalamocortical slice illustrating thalamic stimulation and cortical region. (*B*) Representative single 2D VSDI frames comparing the dynamic properties of the thalamocortical activity in WT (*Upper*) and α-1A KO (*Lower*) mice before and after application of 2 μM Aga-TK or 5 μM Cono-GVIA. (*C*) Spatiotemporal patterns of activation resulting from electrical stimulation of the white matter (WM) at 40 Hz. VSDI for both WT and α-1A KO cortical slices are shown. The cortex is positioned such that layer 1 is on the top and layer 6 is on the bottom. (*D*) 3D profiles of the cortical VSDI activity along layer 4 (see dotted lines in *C*) produced by a 40-Hz train of eight stimuli (white dotes). The set of profiles illustrate the difference in lateral spread of activity between slices from WT (*Left*) and α-1A KO (*Right*) mice.

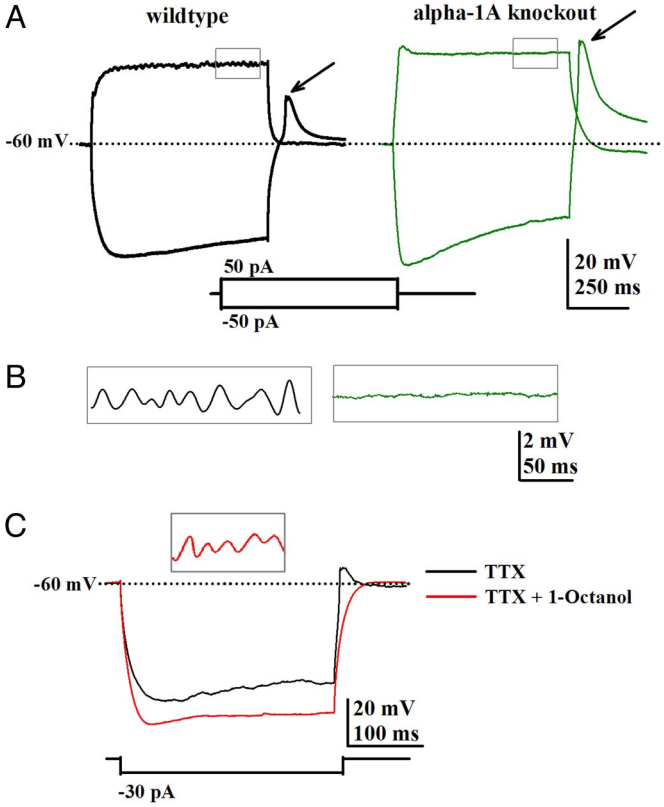

Fig. 2. γ-Oscillations in VB thalamic nucleus neurons are absent in KO mice. (*A*) Patch recordings from VB neurons using both high-potassium pipette solution and 2 μM Tetrodotoxin (TTX) showing the response to both depolarizing and hyperpolarizing pulses in slices from WT (*Left*, black traces) and KO (*Right*, green traces) mice. Note that the rebound spike (mediated by T-type calcium currents) was larger in VB neurons from the KO mice. (*B*) Magnified traces from the area detailed in *A* showing a representative portion of the recording and oscillations only in WT mice. (*C*) Representative patch recordings in the presence of 50 μM 1-Octanol (red lines) during hyperpolarizing pulses showing a clear increment in membrane resistance and no rebound spike after the pulse in WT slice. (*Inset*) γ-Band oscillations were unchanged in the presence of 1-Octanol.

following toxins were applied to the cortex by using a micropipette to selectively block P/Q-, N-, or R-type calcium channels: 2 μM ω-Agatoxin-TK (Aga-TK), 5 μM ω-Conotoxin-GVIA (Cono-GVIA), or 1 μM SNX-482, respectively, while blocking inhibitory synaptic transmission with GABA-A and GABA-B receptor blockers picrotoxin (20 μM) and SCH50911 (30 μM).

The patterns of VSDI fluorescence for single stimuli were similar in slices from both WT and KO mice. Thalamic VB stimulation resulted in the clear activation of both basal ganglia (caudate/putamen) and somatosensory cortex as previously described (ref. 32 and data not shown).

We next examined the type of calcium channels that supported excitatory thalamocortical synaptic transmission in the absence of the P/Q channels. A 2D VSDI signal elicited in a thalamocortical slice by thalamic VB nuclear stimulation (Fig. 1*A*) shows activation of both the thalamus and cortex in WT (Fig. 1*B Upper*) and KO (Fig. 1*B Lower*) mice.

Aga-TK (Fig. 1*B*) abolished thalamocortical activation in slices from WT mice (*Upper*), but did not affect the profiles of excitatory transmission in slices from KO mice (*Lower*). By contrast, Cono-GVIA (Fig. 1*B*) had no effect on the WT response (*Upper*), but blocked thalamocortical activation in the α-1A KO mice (*Lower*). Blocking R-type calcium channels with SNX-482 had no effect on KO thalamocortical activity (n = 6 slices) (data not shown).

These results indicate that N-type calcium channels were able to mediate excitatory synaptic transmission in the thalamocortical system when P/Q channels were not available, maintaining the magnitude of the VSDI signals.

Cortical inhibitory interneurons exhibit intrinsic oscillatory activity in the γ-band frequency range (33) and shape cortical VSDI signals into ≈1-mm-wide columns (31). To determine whether this process occurred with these KO mice, we compared the effects of 40-Hz white matter stimulation in WT and KO mice of the same age (n = 5 slices) (Fig. 1*C*). In WT mice (Fig. 1*D Left*), a sequence in response to eight subsequent 40-Hz stimuli showed a columnar pattern of cortical activity. However, in slices from KO littermates, the 40-Hz stimulation activated a wider area of cortex, with no reduction in the amplitude of VSDI signals (Fig. 1*D Right*). Indeed, the lateral spread of cortical activation in layer 4 was more than twice that of slices from WT mice.

Given this finding, it was important to determine whether thalamic neurons have the same intrinsic properties as WT mice when P/Q VGCC are absent. Of particular interest were the presence of LVA spikes and the generation of subthreshold γ-band (≈40-Hz) oscillations in VB neurons (13). Patch recordings of VB neurons showed clear γ-band oscillations in slices from WT mice (n = 10 slices, n = 2 WT mice) (Fig. 2*A*, black trace enlarged in Fig. 2*B*), but not from KO mice (n = 7 slices, n = 4 KO mice) (Fig. 2*A*, green trace enlarged in Fig. 2*B*), recorded in the presence of 2 μM Tetrodotoxin and high-potassium intracellular patch solution. No such oscillations were observed over a wide range of membrane potentials (−50 to −10 mV) in slices from the KO mice.

Low-threshold rebound calcium spikes observed after hyperpolarizing pulses (e.g., mediated by T-type or Ca_V3 calcium channels) were more robust in slices from KO mice (Fig. 2*A*,

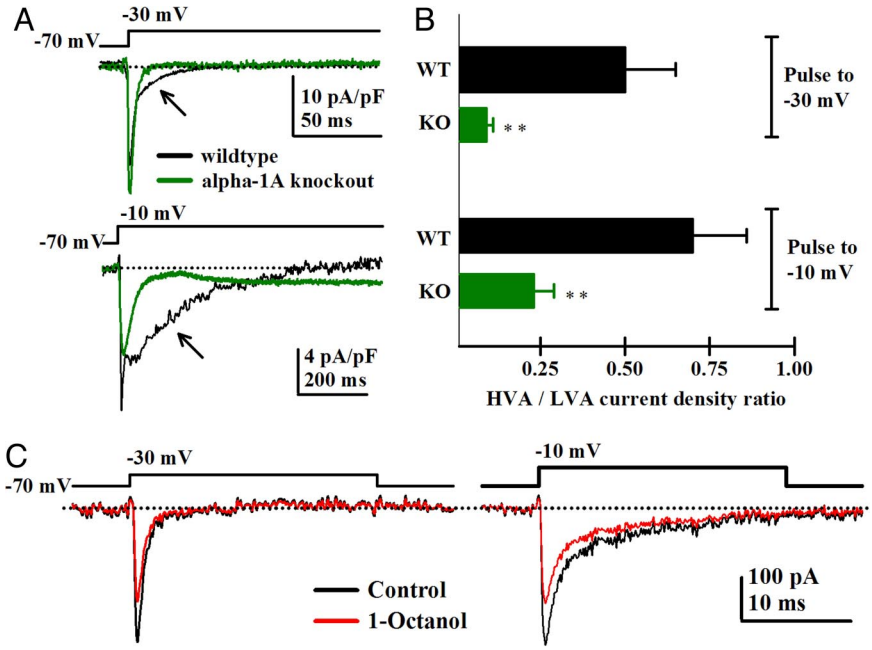

Fig. 3. Increased current density of T-type low-voltage-activated channels in VB neurons from KO mice. (*A*) Representative calcium currents traces recorded with a high-cesium pipette solution at −30 and −10 mV holding potentials for WT (black lines) and KO neurons (green lines). After the fast (T-type-mediated VGCC) component, a small HVA current was observed in WT neurons at −30 mV (black arrow). No HVA current was seen in KO neurons. The current units were pA/pF to standardize current amplitude for different sized cells (due to animals of different ages). (*B*) Bar graph showing the mean ratio of LVA- and HVA-activated currents for WT (black bars) and KO neurons (green bars) for −30- and 10-mV holding potentials (**, $P < 0.02$, Student's *t* test). (*C*) Representative calcium currents elicited at −30 mV (*Upper*) and −10 mV (*Lower*) from a WT VB neuron before (black traces) and after (red traces) application of 10-μM 1-Octanol. Note that 1-Octanol selectively blocked the peak of the fast, T-type, but not the steady-state, P/Q-type calcium current.

green trace, arrow) than in slices from WT mice (Fig. 2*A*, arrow); 50 μM C_2–C_{10} alkyl alcohol, 1-Octanol blocked the rebound spike in slices from both WT and KO mice, leaving the subthreshold γ-band oscillations unchanged (Fig. 2*C*, red traces, representative WT example). Thalamic neurons in slices from WT mice ($n = 4$ neurons, $n = 1$ WT animal) generated γ-band oscillations in the presence of 1-Octanol (Fig. 2*C Inset*), reinforcing the fact that the presence of P/Q-type and not T-type channels were decisive in generating thalamocortical γ-band oscillations in these animals.

We quantified the ratio of high- and low-voltage-activated calcium currents by patch clamping single thalamic VB neurons in slices from both WT and KO mice by using a high-cesium intracellular pipette solution. Voltage steps to −10 and −30 mV were used to compare the maximum peak amplitude of the high-threshold (HVA) and LVA calcium currents, respectively. Representative averaged currents from WT (black traces) and KO (green traces) VB neurons are shown in Fig. 3*A*. At −30 mV, a fast T-type, VGCC-mediated current was recorded from neurons in slices from both types of mice, but only WT neurons presented a small component of HVA current (Fig. 3*A*, black trace, arrow). This current was blocked by Aga-TK, thus corresponding to the activation of a small P/Q-type HVA current component ($n = 2$ VB neurons) (data not shown). Consistently, at −10 mV, a robust HVA component was observed, whereas the LVA component decreased for both WT and KO neurons (Fig. 3*A Lower*). The HVA calcium current amplitude was still smaller in KO neurons than in WT neurons (Fig. 3*A Lower*, arrows). The mean ratio of HVA to LVA currents (HVA/LVA) was significantly smaller at both holding potentials for KO neurons (Fig. 3*B*, green) than for WT neurons (Fig. 3*B*, black). At a −30-mV holding potential, the HVA/LVA ratio was 0.50 ± 0.15 ($n = 12$ neurons, $n = 6$ KO mice) for WT and 0.09 ± 0.02 ($n = 13$ neurons, $n = 4$ WT mice; $P = 0.012$) for KO neurons. At a holding potential of −10 mV for WT, neurons presented a mean ratio of 0.7 ± 0.16 ($n = 12$ neurons, $n = 4$ WT mice), whereas only a 0.23 ± 0.06 ratio ($n = 13$ neurons, $n = 6$ KO animals; $P = 0.013$) was observed for KO neurons. In the presence of 10 μM 1-Octanol (Fig. 3*C*, red traces), LVA (Fig. 3*C Left*), but not HVA, currents (slow component) (Fig. 3*C Right*) were reduced as previously described (2).

EEGs were recorded from freely moving WT and KO mice by using epidural electrodes. The EEGs of WT mice had a normal pattern of activity at both low and high frequencies (Fig. 4*A*, black trace). The EEGs of KO mice had 3- to 5-Hz repetitive spike-and-wave discharges (SWDs) (Fig. 4*A*, red traces), which are compatible with an absence status. During SWD activity, these animals were immobile and did not show the responsive behavior typical of animals of comparable age as previously described (30). A histogram quantified the absolute power in four different frequency ranges obtained from both WT and KO mice (Fig. 4*B*), which excluded the large portion of SWD activity in the KO animals. The graph demonstrates the fundamental difference in the spontaneous electrical activity of these two genotypes, showing that the power of low-, but not high-frequency ranges were exacerbated. δ-Band and θ-band power was 500% and 400% larger in KO mice, respectively, [ANOVA comparison between genotypes, $F(1,12) = 16.83$, $P = 0.001$], whereas power in the γ-band was reduced [ANOVA, $F(1,12) = 13.78$, $P = 0.003$]. There were no differences between KO and WT mice in the α-band.

Finally, a 0.2 mg/kg dose of 1-Octanol was administered i.p. to the animals to determine the effect of reducing T-type VGCC on the EEG activity of both WT and KO mice after the removal of all EEG segments containing SWD components. Thirty to 60 min after a single injection, 1-Octanol significantly reduced the low-frequency power (75 ± 9% reduction at 3–5 Hz) in the KO mice, with no change in EEG activity in WT mice (Student's *t*

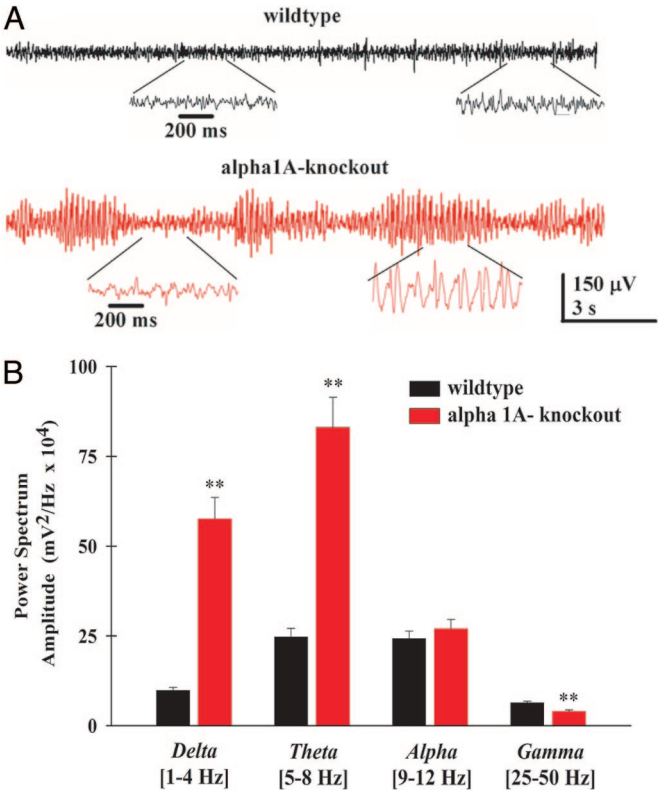

Fig. 4. Absence of γ-band activity in EEG recordings from KO mice. (*A*) (*Upper*) Representative EEG traces from a freely moving WT animal showing the typical low-amplitude pattern of an awake animal with the presence of both low- and high-frequency activity (expanded in *Inset*). (*Lower*) EEG traces from a freely moving KO mouse showing repetitive SWD (expanded in *Inset*). (*B*) Histogram of the mean relative power spectrum for WT ($n = 5$) and KO ($n = 7$) mice. The ranges of frequencies used are shown in brackets under the *x* axis. Note the significant increase in δ- and θ-bands and the decrease in α- and γ-bands in the KO mice (**, $P < 0.01$, ANOVA comparison between groups).

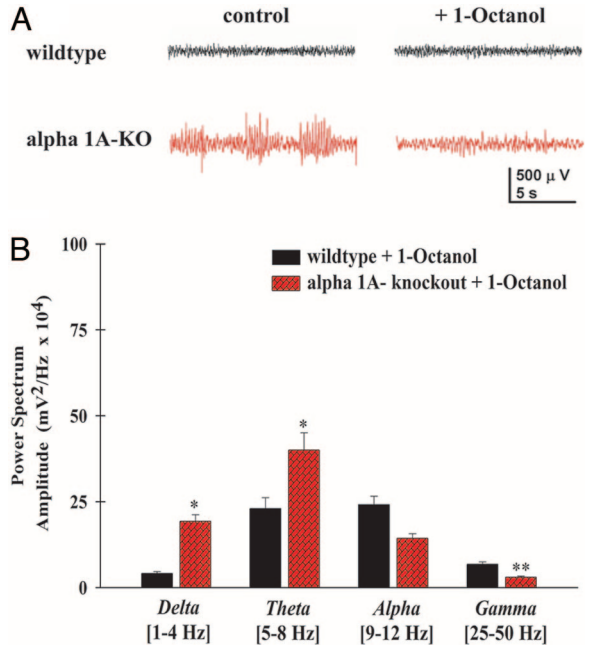

Fig. 5. The alkyl alcohol, 1-Octanol, reduces low-frequency EEG activity, leaving α-1A KO mice in a coma-like state. (*A*) Representative EEG traces from a freely moving KO animal before (*Left*) and after (*Right*) a single 0.2 mg/kg injection of 1-Octanol i.p. in WT (black traces) and KO (red traces). Note that 1-Octanol reduced the amplitude of SWD activity. (*B*) Bar graph of the mean power for both WT ($n = 5$) and KO mice ($n = 4$) showing the effect of 1-Octanol on power in four frequency bands ($P < 0.05$, ANOVA comparison between groups).

test, $P < 0.05$) (Fig. 5*A*, compare *Left* and *Right*). The KO animals were immobile and in a coma-like state during the entire recording period after 1-Octanol injection. This result was reversible, and the animals returned to their default absence status after 12 h ($n = 4$ KO mice). The mean power spectrum of the EEG was reduced by 80% in the δ, θ, and α ranges [ANOVA cross-comparison between genotypes and treatment with post hoc Fisher LSD between Octanol/Tween 80, δ- and θ-bands, $F(1,12) = 8.17, P = 0.014$; α-bands, $F(1,12) = 4.82, P = 0.04$] whereas the reduction in the γ-band component was not significant (compare Fig. 4*B* with Fig. 5*B*).

It is interesting to note that the power in the γ-band increased in the presence of 1-Octanol, although this increase was not statistically significant. There was a significant difference, however, in γ-band power between KO and WT mice after Octanol [$P < 0.05$, ANOVA comparison genotype with post hoc Fisher LSD, $F(1,12) = 13.7, P = 0.0029$] (Fig. 5*B*). By contrast, the same low dose of 1-Octanol did not affect the EEG or behavior of WT mice ($n = 4$).

We can conclude from this last set of experiments that P/Q calcium channels are essential in the generation of γ-band EEG activity, and that the deep cognitive deficit in KO mice is not simply due to the absence status accompanying the increased T-type channels activity. Rather, the inability of the brain to generate γ-band activation, apparently related to the absence of P/Q-type channels and the specific molecular cohort in the cytosolic space associated with these channels, could be the dominant component.

Discussion

These findings show that, although N-type VGCC can replace some functional properties of P/Q-type VGCC, quite different patterns of activity result from this rescued synaptic transmission. Indeed, although synaptic transmission is implemented by the N-type channel substitution, the system at both the neuronal and circuit levels demonstrates different dynamic properties. It is not just the entry of calcium that is the determinant of such dynamic properties, but rather that the intracellular machinery associated with the given channel types is a fundamental variable. Moreover, because the block of T-type VGCC (by using 1-Octanol), which produced a marked reduction of low-frequency activity, did not result in an increase in γ-band power in the KO mice and resulted in animals being in a coma-like state, we can associate P/Q-type channel activity with cognitive brain function.

At the neuronal level, the absence of subthreshold γ-band oscillations was clear in KO thalamic neurons, although these are a basic characteristic of such neurons (13) among many vertebrate subgroups (22). At the same time, larger T-type-mediated activity in thalamic neurons from KO mice was encountered. Considering that the thalamocortical dysrhythmia syndrome has been associated with a set of neurological and/or psychiatric conditions arising from abnormal rhythmicity in particular components of the thalamocortical circuit (caused by an increase of low-frequency oscillatory activity) (23, 24), these results are of a great relevance. Indeed, α-1A KO mice may be considered as an animal model of the thalamocortical dysrhythmia syndrome.

Previous studies have shown that mutations of specific subunits, as well as the genetic deletion of the P/Q-type calcium channel, are able to induce abnormally large T-type current density (30, 34). In the thalamocortical system as a whole, such abnormal rhythmicity interferes with normal communication among and between different thalamocortical pathways, impair-

ing the motor and cognitive functions of the entire system. The current density changes of T-type channels do not explain the generation of SWDs in EEG recordings (30). Indeed, the elimination and mutation of P/Q-type channels induced higher current densities of T-type channels in thalamic neurons (34). Curiously, similar increments in T-type current density have been described when the neurotransmitter-release machinery is affected (SNAP-25-deficient *Coloboma* mutant) (35).

Because the prevalent low-frequency EEG activity observed in KO mice is likely to be due to an increase in the number of T-type calcium channels, the possibility was considered that γ-band activity could be manifested if T channel were to be blocked pharmacologically using 1-Octanol. Our results showed a significant reduction of EEG power at low frequencies in KO mice even when1-Octanol was administered at a low dose (36). However, 1-Octanol did not augment the low-level γ-band activity that was originally present (probably related to an emergent 40-Hz activity from cortical interneurons) (33), and the animals were in a coma-like state.

In conclusion, the physiopathology observed in animals in which P/Q channels were genetically removed must be related to the central role of those channels in the thalamocortical system. Indeed, neither the substitution of N-type channels nor the blocking of T-type channels with 1-Octanol was important to recover consciousness (i.e., the global brain state with its characteristic thalamocortical γ-band activity) in α-1A KO mice.

Materials and Methods

Animals. $Ca_V2.1$-null (i.e., α-1A KO) mice and their littermate controls were generated by mating mice heterozygous for the $Ca_V2.1$ from C57BL/6J background. Animal care and handling were carried out following New York University School of Medicine Center guidelines.

Obtaining Slices. P7 to P21 WT and $Ca_V2.1$-null mice were anesthetized with 120 mg/kg pentobarbital i.p. (Nembutal) and decapitated, and 350 to 400 μM thalamocortical slices were obtained as previously described (32). When needed 300- to 450-μm coronal cortical slices were collected from the somatosensory barrel cortex (31). Slices were produced while the brain was submerged in a chamber containing a chilled low-sodium/high-sucrose artificial cerebrospinal fluid (aCSF) solution (248 mM sucrose, 26 mM $NaHCO_3$, 1.25 mM NaH_2PO_4, 5 mM KCl, 2 mM $MgSO_4$, 0.5 mM $CaCl_2$, and 10 mM glucose) and aerated with 95% O_2/5% CO_2 (pH 7.4). Then 375- to 450-μm slices were allowed to recover in an incubation chamber at 35°C for at least 30 min. The chamber contained a continuously oxygenated combination of 50% low-sodium/high- sucrose aCSF and 50% normal aCSF [124 mM NaCl, 5 mM KCl, 1.25 mM KH_2PO_4, 26 mM $NaHCO_3$, 1.2 mM $MgCl_2$, 2.4 mM $CaCl_2$, and 10 mM glucose (pH 7.4)].

Whole-Cell Patch Recordings. Patch recordings were made at 35°C in normal aCSF. Patch electrodes were made from borosilicate glass and had resistances of 3–10 MΩ when filled with either a high-potassium intracellular solution [130 mM $KMeSO_3$, 10 mM NaCl, 10 mM Hepes, 1 mM EGTA, 4 mM Mg-ATP, 0.4 mM Na-GTP, 2 mM $MgCl_2$, 10 mM sucrose, and 10 mM phosphocreatine (pH 7.3, 290 mOsm)] or a high-cesium/QX314 intracellular solution [120 mM $CsMeSO_3$, 8 mM NaCl, mM Hepes, 5 mM EGTA, 10 mM TEA-Cl, 4 mM Mg-ATP, 0.5 mM mM GTP, and 7 mM phosphocreatine (pH 7.3, 290 mOsm)]. Before patch recordings were performed, 2 mg/ml biocytin was included in the intracellular solution to permit characterization of the recorded neuron's morphology by using the ABC kit-DAB method. Neurons were recorded by using a MultiClamp 700 amplifier (Axon Instruments, Union City, CA; Molecular Devices, Sunnyvale, CA) in combination with the PCLAMP 10.0 software (Axon Instruments, Molecular Devices). Data were filtered at 5 kHz, digitized, and stored for off-line analysis; and 8–25 MΩ access resistance was continuously monitored during the experiments.

Recording and Analysis of VSDI Signals. The VSDI apparatus comprised a 12-volt halogen light source, a 515 ± 35-nm filter, a dichroic mirror, and a 5× microscope objective. The slice was stained with 25 μg/ml voltage-sensitive dye di-4ANEPPS (Molecular Probes, Eugene, OR). The emitted fluorescent light was monitored with a CCD camera MICAM Ultima (1 msec per frame vs. 0703; BrainVision, Tokyo, Japan). Optical recordings were analyzed off-line by using BrainVision analyzer software. Changes in membrane potential were evaluated as DF/F (F-Fo/F, where Fo is the base fluorescence level).

The optical signals were displayed with the maximum amplitude set to the maximum red intensity of the CMYK scale. Bipolar electrical stimulation (at twice threshold) was delivered to either the VB thalamic nucleus or white matter for the study of thalamocortical or corticothalamic responses, respectively.

EEG Recordings and Spectral Power Analysis. Differential EEG recordings were performed as described previously (30). Two- to 3-week-old mice were anesthetized with 75 mg/kg Ketamin and 5 mg/kg Xylazin s.c. A local s.c. injection of lidocaine was delivered to the skin over the scalp before it was opened and retracted. An epidural EEG electrode was implanted over the temporal lobe, and a ground electrode was implanted over the occipital region. A head mount was secured by using dental cement, and the mice were allowed to recover for at least 24 h. EEG signals were amplified (model 1700; A-M Systems, Carlsborg, WA) and digitized at a sampling frequency of 200 μsec. Data were acquired by using a PCLAMP10.0 program (Axon Instruments, Molecular Devices). During the recording, 2- to 40-Hz random acoustic stimuli were delivered to keep the animals alert. Spectral power was calculated by Fourier transformation (Hamming window). The mean spectral power was calculated from at least 60 artifact-free, 2-sec epochs for each animal. The effects of 1-Octanol on the EEG were studied 30–60 min after injection of 0.2 mg/kg 1-Octanol i.p. as described in ref. 36.

Pharmacological Reagents. Drugs were applied locally by pressure injection through a pipette. Drugs were purchased from Sigma–Aldrich (St. Louis, MO). The voltage-sensitive dye di-4ANEPPS was purchased from Molecular Probes.

Statistical Analysis. Sigmaplot 10.0 (Systat, San Jose, CA) software was used for statistical comparisons. Statistics were performed with two-tailed unpaired and paired Student's t tests for both imaging and patch recordings. EEG power for frequency bands was compared by using ANOVA analysis. Differences were considered significant if $P < 0.05$. Population statistics are presented here as mean ± SEM.

This work was supported by National Institutes of Health Grant NS13742 (to R.R.L.), the Korea Research Foundation, and Korean Government Ministry of Education and Human Resources Development Grant KRF-2005-213-E00003 (to S.C.).

1. Llinás R, Hess R (1976) *Proc Natl Acad Sci USA* 73:2520–2523.
2. Llinas R (1988) *Science* 242:1654–1664.
3. Catterall WA (1998) *Cell Calcium* 24:307–323.
4. Katz B, Miledi R (1965) *Proc R Soc Lond B Biol Sci* 161:496–503.
5. Llinas R, Sugimori M, Lin JW, Cherksey B (1989) *Proc Natl Acad Sci USA* 86:1689–1693.

6. Hillman D, Chen S, Aung TT, Cherksey B, Sugimori M, Llinas R (1991) *Proc Natl Acad Sci USA* 88:7076–7080.
7. Uchitel OD, Protti DA, Sanchez V, Cherksey BD, Sugimori M, Llinás R (1992) *Proc Natl Acad Sci USA* 89:3330–3333.
8. Kim DK, Catterall WA (1997) *Proc Natl Acad Sci USA* 94:14782–14786.
9. Zhong H, Yokoyama CT, Scheuer T, Catterall WA (1999) *Nat Neurosci* 2:939–941.
10. Bergsman JB, Tsien RW (2000) *J Neurosci* 20:4368–4378.
11. Singer W (1998) *Phil Trans R Soc Lond B* 353:1829–1840.
12. Llinas R, Ribary U, Contreras D, Pedroarena C (1998) *Phil Trans R Soc Lond B 353:1841–1849.*
13. Pedroarena C, Llinas R (1997) *Proc Natl Acad Sci USA* 94:724–728.
14. Luo M, Perkel DJ (1999) *J Neurosci* 19:6700–6711.
15. Rhodes PA, Llinás R (2005) *J Physiol* 565:765–781.
16. Iwasaki S, Momiyama A, Uchitel OD, Takahashi T (2000) *J Neurosci* 20:59–65.
17. Ali AB, Nelson C (2006) *Cereb Cortex* 16:386–393.
18. Caddick SJ, Wang C, Fletcher CF, Jenkins NA, Copeland NG, Hosford DA (1999) *J Neurophysiol* 81:2066–2074.
19. Sasaki S, Huda K, Inoue T, Miyata M, Imoto K (2006) *J Neurosci* 26:3056–3065.
20. Pietrobon D (2005) *Curr Opin Neurobiol* 15:257–265.
21. Steriade M, Llinas RR (1988) *Physiol Rev* 68:649–742.
22. Llinas RR, Steriade M (2006) *J Neurophysiol* 95:3297–3308.
23. Llinas RR, Ribary U, Jeanmonod D, Kronberg E, Mitra PP (1999) *Proc Natl Acad Sci USA* 96:15222–15227.
24. Llinas R, Urbano FJ, Leznik E, Ramirez RR, van Marle HJ (2005) *Trends Neurosci* 28:325–333.
25. Jun K, Piedras-Renteria ES, Smith SM, Wheeler DB, Lee SB, Lee TG, *et al.* (1999) *Proc Natl Acad Sci USA* 96:15245–15250.
26. Urbano FJ, Piedras-Renteria ES, Jun K, Shin HS, Uchitel OD, Tsien RW (2003) *Proc Natl Acad Sci USA* 100:3491–3496.
27. Pagani R, Song M, McEnery M, Qin N, Tsien RW, Toro L, Stefani E, Uchitel OD (2004) *Neuroscience* 123:75–85.
28. Inchauspe CG, Martín FJ, Forsythe ID, Uchitel OD (2004) *J Neurosci* 24:10379–10383.
29. Cao YQ, Piedras-Renteria ES, Smith GB, Chen G, Harata NC, Tsien RW (2004) *Neuron* 43:387–400.
30. Song I, Kim D, Choi S, Sun M, Kim Y, Shin HS (2004) *J Neurosci* 24:5249–5257.
31. Contreras D, Llinas R (2001) *J Neurosci* 21(23):9403–9413.
32. Llinas RR, Leznik E, Urbano FJ (2002) *Proc Natl Acad Sci USA* 99:449–454.
33. Llinas RR, Grace AA, Yarom Y (1991) *Proc Natl Acad Sci USA* 88:897–901.
34. Zhang Y, Mori M, Burgess DL, Noebels JL (2002) *J Neurosci* 22:6362–6371.
35. Zhang Y, Vilaythong AP, Yoshor D, Noebels JL (2004) *J Neurosci* 24:5239–5248.
36. Sinton CM, Krosser BI, Walton KD, Llinas RR (1989) *Pflügers Arch* 414:31–36.